

# Distortion-Aware Linear Precoding for Massive MIMO Downlink Systems with Nonlinear Power Amplifiers

Sina Rezaei Aghdam, *Member, IEEE*, Sven Jacobsson,  
Ulf Gustavsson, Giuseppe Durisi, *Senior Member, IEEE*,  
Christoph Studer, *Senior Member, IEEE*, Thomas Eriksson

## Abstract

We introduce a framework for linear precoder design over a massive multiple-input multiple-output downlink system and in presence of nonlinear power amplifiers (PAs). By studying the spatial characteristics of the distortion, we demonstrate that conventional linear precoding techniques steer nonlinear distortions in the direction of the users. We show that, by taking into account PA nonlinearity characteristics, one can design linear precoders that reduce, and in single-user scenarios, even remove completely the distortion transmitted in the direction of the users. This, however, is achieved at the price of a considerably reduced array gain. To address this issue, we present precoder optimization algorithms which simultaneously take into account the effects of array gain, distortion, multiuser interference, and receiver noise. Specifically, we derive an expression for the achievable sum rate and propose an iterative algorithm that attempts to find the precoding matrix maximizing this expression. Moreover, using a model for PA power consumption, we propose an algorithm that attempts to find the precoding matrix minimizing the consumed power for a given minimum achievable sum rate. Our numerical results demonstrate that the proposed distortion-aware precoding techniques yield considerable improvements in terms of spectral and energy efficiency compared to conventional linear precoding techniques.

Sina Rezaei Aghdam, Giuseppe Durisi and Thomas Eriksson are with the Department of Electrical Engineering, Chalmers University of Technology, 41296 Gothenburg, Sweden. (e-mails: {sinar, durisi, thomase}@chalmers.se).

Sven Jacobsson and Ulf Gustavsson are with Ericsson Research, 41756 Gothenburg, Sweden. (e-mails: {sven.jacobsson, ulf.gustavsson}@ericsson.com).

Christoph Studer is with the Department of Information Technology and Electrical Engineering, ETH Zürich, Zürich, Switzerland. (e-mail: studer@ethz.ch).

The work of Sina Rezaei Aghdam and Thomas Eriksson was performed within the strategic innovation program “Smarter Electronics Systems”, a common venture by VINNOVA, Formas, and Energimyndigheten. The work of Sven Jacobsson was supported in part by the Swedish Foundation for Strategic Research under grant ID14-0022, and by VINNOVA within the competence center ChaseOn.

This paper was presented by part at IEEE ICC 2019 Workshop on millimeter-wave communications for 5G and B5G [1].

### Index Terms

Massive multiple-input multiple-output, nonlinear power amplifier, in-band distortion, linear pre-coding, energy efficiency, and out-of-band emission.

## I. INTRODUCTION

Massive multiple-input multiple-output (MIMO) technology has already proven its large potential for enhancing spectral efficiency in fifth generation (5G) cellular networks [2]. The key idea is to equip base stations with many individually controllable antennas to serve multiple users over the same time-frequency resource via spatial multiplexing. To make massive MIMO commercially viable, the base station should be deployed using low-complexity and inexpensive hardware. Dealing with hardware impairments is therefore one of the main challenges in making massive MIMO practically feasible, see, e.g., [3]–[6].

Low-cost and low-precision hardware can lead to different impairments such as nonlinear amplification, quantization noise, phase noise, and in-phase/quadrature (I/Q) imbalance. How to model these impairments and how to evaluate the resulting performance loss have been the subject of extensive investigations. As far as modeling is concerned, two approaches are typically followed in the literature.

The first approach deals with the characterization of a single (or pre-dominant) hardware impairment which is modeled using accurate parametric models. For example, the impact of power amplifier (PA) nonlinearities on the performance of multi-antenna systems has been investigated in [7]–[9]. The work in [10] characterizes the performance of millimeter-wave multi-antenna systems, in terms of spectral and energy efficiency, in the presence of PA nonlinearities and crosstalk. The impact of other hardware impairments such as phase noise, I/Q imbalance, and quantization has been investigated in, e.g., [11]–[13].

The second approach consists of evaluating the joint effect of multiple hardware impairments; see, e.g., [4], [14]–[16]. In these works, the aggregate distortion is simply modeled as an additive Gaussian noise that is often assumed uncorrelated across the antenna array. While spatially uncorrelated models of the distortion may be accurate in some scenarios (see, e.g., [16]), they are typically unsuitable to characterize the massive MIMO downlink with multiuser precoding [17], [18]. Aggregate hardware impairment models capturing the inherent spatial correlation of the distortion are therefore of high practical importance. One example of such an aggregate

hardware impairment model has been introduced in [19]. This model captures the individual distortions caused by nonlinear amplifiers as well as phase noise and quantization noise.

In scenarios with spatially-correlated distortion, knowledge on the covariance matrix of the distortion can be leveraged to enhance communication performance. For instance, distortion-aware linear receivers [20], [21] have shown improved performance with respect to conventional linear receivers by (partially) suppressing the distortion at the price of a reduced array gain. Distortion-aware channel estimation techniques have also been recently proposed [22]. These techniques are able to reduce the estimation error by exploiting the statistical characteristics of the impairments.

In this work, we focus on a downlink multiuser MIMO system with nonlinear PAs at the base station. We demonstrate that by incorporating the knowledge of the distortion correlation in the linear precoder design, one can suppress the nonlinear distortion in the direction of the users, achieving considerable gains compared to conventional linear precoders. More specifically, the main contributions of this paper are as follows:

- We study the directivity of the nonlinear PAs' distortion in a single-user setup. We model the nonlinear PAs using memoryless polynomials and analytically derive linear precoders that can null the distortion in the direction of the user at the cost of considerably reducing array gain to the user and increasing radiation in unwanted directions.
- In view of the fact that the precoders nulling the distortion in the direction of the users are not necessarily favorable solutions in many scenarios, e.g., at low-to-moderate signal-to-noise ratio (SNR), we propose a linear precoder optimization framework which simultaneously takes into account the effect of the distortion, the array gain and, the multiuser interference. We utilize Bussgang's theorem [23] to decompose the distorted transmit signal into a linear and an uncorrelated distortion term. We then derive a lower bound on the sum rate and propose an iterative procedure, which we refer to as distortion-aware beamforming (DAB). This procedure computes a linear precoder that maximizes the sum rate under an average total power constraint. We show that the DAB precoder is able to achieve considerable gains in terms of spectral efficiency, as compared to conventional distortion-unaware precoding techniques, such as maximal-ratio transmission (MRT) and zero-forcing (ZF).
- We generalize our framework by further considering the consumed power in the PAs. We adopt a simple PA power consumption model and formulate a precoder optimization framework that minimizes the consumed power under a constraint on the minimum required

sum rate. We then propose an iterative algorithm to approximately solve this optimization problem. We refer to the output of this iterative algorithm as the energy-efficient DAB (EE-DAB) precoding matrix.

- We conduct extensive numerical experiments to evaluate the efficacy of the proposed framework in a variety of scenarios. We quantify the improvements that can be achieved by DAB and EE-DAB in terms of spectral and energy-efficiency, respectively, compared to conventional distortion-unaware precoding techniques. Moreover, we study the out-of-band radiation and demonstrate that the proposed precoder optimization framework can be utilized to enforce that spectral regrowth due to nonlinear PAs stays below given limits.

*Paper Outline:* The rest of the paper is organized as follows. The system model is described in Section II. In Section III, we utilize Bussgang's theorem to decompose the PA output into a linear term and an uncorrelated distortion term and use this decomposition to derive an expression for the achievable sum rate. We analyze the directivity of nonlinear distortion under different choices of linear precoders in Section IV. Our proposed distortion-aware precoder optimization techniques, i.e., DAB and EE-DAB, are detailed in Sections V and VI, respectively. Numerical examples that demonstrate the efficacy of the proposed precoders are given in Section VII and the paper is concluded in Section VIII.

*Notation:* Lowercase and uppercase boldface letters denote vectors and matrices, respectively. The superscripts  $(\cdot)^*$ ,  $(\cdot)^T$ , and  $(\cdot)^H$  denote complex conjugate, transpose, and Hermitian transpose, respectively. We use  $\mathbb{E}[\cdot]$  to denote expectation. We use  $\|\mathbf{a}\|$  to denote the  $\ell_2$ -norm of the vector  $\mathbf{a}$ . The  $M \times M$  identity matrix is denoted by  $\mathbf{I}_M$  and the  $M \times M$  all-zeros matrix is denoted by  $\mathbf{0}_{M \times M}$ . We use  $\mathbf{A} \odot \mathbf{B}$  to denote the Hadamard (entry-wise) product of two equally-sized matrices  $\mathbf{A}$  and  $\mathbf{B}$ ;  $\text{tr}(\cdot)$  denotes the trace of a matrix. Furthermore,  $\text{diag}(\mathbf{a})$  represents a diagonal matrix that contains the elements of the vector  $\mathbf{a}$  on its diagonal, and  $\text{diag}(\mathbf{A})$  is the main diagonal of a square matrix  $\mathbf{A}$ . The element-wise magnitude of a matrix  $\mathbf{A}$  is represented by  $|\mathbf{A}|$ . We use  $\angle a$  to denote the angle of the complex number  $a$ . The distribution of a circularly-symmetric complex Gaussian random vector with covariance matrix  $\mathbf{C} \in \mathbb{C}^{M \times M}$  is denoted by  $\mathcal{CN}(\mathbf{0}_{M \times M}, \mathbf{C})$ . Finally, we use  $\mathbb{1}_{\mathcal{A}}(a)$  to denote the indicator function, which is defined as  $\mathbb{1}_{\mathcal{A}}(a) = 1$  for  $a \in \mathcal{A}$  and  $\mathbb{1}_{\mathcal{A}}(a) = 0$  for  $a \notin \mathcal{A}$ .

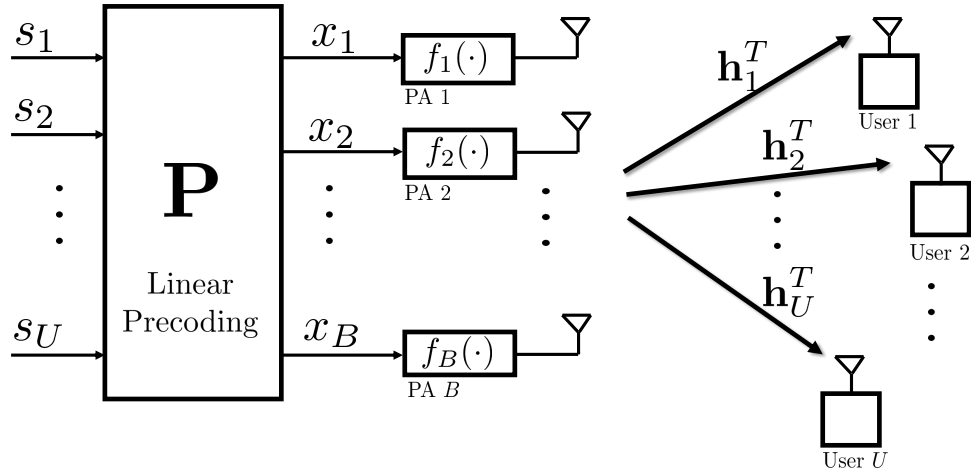


Fig. 1. Massive MIMO downlink with linear precoding and nonlinear PAs at the transmitter.

## II. SYSTEM MODEL

We consider a massive MIMO downlink scenario as depicted in Fig. 1. The base station is equipped with  $B$  antennas and serves  $U$  single-antenna users over the same time-frequency resource. Each antenna is connected to a nonlinear PA, which introduces distortion into the transmit signal.

### A. Channel Input-Output Relationship

The received signal at the  $u$ th user is given by

$$y_u = \mathbf{h}_u^T f(\mathbf{x}) + w_u, \quad (1)$$

for  $u = 1, \dots, U$ , where  $\mathbf{h}_u \in \mathbb{C}^B$  represents the channel between the base station and the  $u$ th user. The function  $f(\mathbf{x}) = [f_1(x_1), \dots, f_B(x_B)]^T$  describes the output of the PAs. Here,  $f_b(\cdot) : \mathbb{C} \rightarrow \mathbb{C}$  characterizes the memoryless nonlinear behavior of the PA at the  $b$ th antenna,  $b = 1, \dots, B$ . We consider linear precoding where the precoded signal is given by  $\mathbf{x} = \mathbf{Ps}$ . Here,  $\mathbf{P} = [\mathbf{p}_1, \dots, \mathbf{p}_U] \in \mathbb{C}^{B \times U}$  denotes the precoding matrix and  $\mathbf{s} = [s_1, \dots, s_U]^T \sim \mathcal{CN}(\mathbf{0}_{U \times U}, \mathbf{I}_U)$  model the transmitted symbols. Finally,  $w_u \sim \mathcal{CN}(0, N_0)$  in (1) is additive white Gaussian noise (AWGN). Throughout the paper, we assume that perfect channel state information (CSI) is known at both the transmitter and the users.

### B. PA Nonlinearity Model

We model the PAs using a polynomial. Specifically, the nonlinear behavior of the  $b$ th PA is modeled by the following  $(2K + 1)$ th order polynomial:

$$f_b(x_b) = \sum_{k=0}^K \beta_{2k+1}^{(b)} x_b |x_b|^{2k} = \beta_1^{(b)} x_b + \beta_3^{(b)} x_b |x_b|^2 + \cdots + \beta_{2K+1}^{(b)} x_b |x_b|^{2K}, \quad (2)$$

for  $b = 1, \dots, B$ , where  $\beta_1^{(b)}, \beta_3^{(b)}, \dots, \beta_{2K+1}^{(b)}$  are complex-valued model parameters that capture both amplitude-to-amplitude modulation (AM/AM) and amplitude-to-phase modulation (AM/PM) distortions [24]. Nonlinear memory effects are typically much weaker than the direct nonlinearities. Therefore, we have neglected them throughout this work and analysis of their impact on precoder design is left for future studies.

### C. PA Power Consumption Model

In order to model the PAs' power consumption, we use the model proposed in [25, Eq. (4)]. Specifically, let us denote the output power from the  $b$ th PA by  $\rho_{\text{tx},b}$  and represent the consumed power at that PA by  $\rho_{\text{cons},b}$ . Then the power efficiency can be expressed as

$$\eta_b = \frac{\rho_{\text{tx},b}}{\rho_{\text{cons},b}}, \quad (3)$$

for  $b = 1, \dots, B$ . Via measurements, the authors in [25] have verified that the following equation accurately describes the power efficiency for a large variety of PAs:

$$\eta_b = \eta_{\max,b} \sqrt{\frac{\rho_{\text{tx},b}}{\rho_{\max,b}}}. \quad (4)$$

Here,  $\eta_{\max,b} \in [0, 1]$  is the maximum power efficiency obtained when  $\rho_{\text{tx},b} = \rho_{\max,b}$ . From (3) and (4), the consumed power at the  $b$ th PA can be expressed as

$$\rho_{\text{cons},b} = \frac{1}{\eta_{\max,b}} \sqrt{\rho_{\text{tx},b} \rho_{\max,b}}, \quad (5)$$

for  $b = 1, \dots, B$  where  $\rho_{\text{tx},b} \leq \rho_{\max,b}$ . In words, the consumed power is proportional to the square root of the output power which is compatible with the results in several other studies, see, e.g., [26, Eq. (6.93)].

### III. BUSSGANG DECOMPOSITION AND SPECTRAL EFFICIENCY

In order to analyze the impact of the PA distortion on the performance of the system, we shall use Bussgang's theorem [23] to decompose the nonlinear signal into a scaled linear term and an uncorrelated distortion term. This allows us to derive a lower bound on the sum rate as a metric for evaluating spectral efficiency.

#### A. Bussgang's Theorem

By applying Bussgang's theorem [23], we can, similarly to, e.g., [10], [19], [20], rewrite the distorted signal  $f(\mathbf{x})$  as

$$f(\mathbf{x}) = \mathbf{G}\mathbf{x} + \mathbf{e}, \quad (6)$$

where the distortion term  $\mathbf{e} \in \mathbb{C}^B$  is uncorrelated with  $\mathbf{x}$ , i.e.,  $\mathbb{E}[\mathbf{x}\mathbf{e}^H] = \mathbf{0}_{B \times B}$ . Furthermore,  $\mathbf{G} \in \mathbb{C}^{B \times B}$  is a diagonal matrix containing the Bussgang gains, whose entries along the diagonal are given by  $[\mathbf{G}]_{b,b} = \mathbb{E}[f(x_b)x_b^*]/\mathbb{E}[|x_b|^2]$  for  $b = 1, \dots, B$ . For the  $K$ th order polynomial model in (2) and for  $\mathbf{x} = \mathbf{P}\mathbf{s}$ , we derive the gain matrix  $\mathbf{G}$  in (6) as a function of the precoding matrix  $\mathbf{P}$  as

$$\mathbf{G}(\mathbf{P}) = \sum_{k=0}^K (k+1)! \mathbf{A}_{2k+1} \text{diag}(\mathbf{C}_\mathbf{x})^k \quad (7)$$

$$= \mathbf{A}_1 \mathbf{I}_B + 2\mathbf{A}_3 \text{diag}(\mathbf{C}_\mathbf{x}) + \dots + (K+1)! \mathbf{A}_{2K+1} \text{diag}(\mathbf{C}_\mathbf{x})^K, \quad (8)$$

where

$$\mathbf{A}_{2k+1} = \text{diag}([\beta_{2k+1}^{(1)}, \dots, \beta_{2k+1}^{(B)}]), \quad (9)$$

for  $k = 1, \dots, K$  and  $\mathbf{C}_\mathbf{x} = \mathbb{E}[\mathbf{x}\mathbf{x}^H] = \mathbf{P}\mathbf{P}^H$  is the input covariance matrix. Using (7) and following a similar approach as in, e.g., [20, Eq. (24)], the covariance matrix of the distortion  $\mathbf{e}$  can be derived as

$$\mathbf{C}_\mathbf{e}(\mathbf{P}) = \sum_{k=0}^K \mathbf{L}_k \mathbf{C}_\mathbf{x} \odot |\mathbf{C}_\mathbf{x}|^{2k} \mathbf{L}_k^H, \quad (10)$$

where

$$\mathbf{L}_k = \frac{1}{\sqrt{k+1}} \sum_{l=k}^K \binom{l}{k} (l+1)! \mathbf{A}_{2l+1} \text{diag}(\mathbf{C}_\mathbf{x})^{l-k}. \quad (11)$$

It can be seen from (10) that when the channel input  $\mathbf{x}$  has correlated elements, the distortion will be spatially correlated. In other words, having off-diagonal elements in  $\mathbf{C}_\mathbf{x}$  (as is, in general,

the case for precoding) leads to off-diagonal elements in the distortion covariance matrix  $\mathbf{C}_e$ .

### B. Achievable Sum Rate

By inserting (6) into (1), the received signal at the  $u$ th user can be written as

$$y_u = \mathbf{h}_u^T \mathbf{G}(\mathbf{P}) \mathbf{p}_u s_u + \sum_{r \neq u} \mathbf{h}_u^T \mathbf{G}(\mathbf{P}) \mathbf{p}_r s_r + \mathbf{h}_u^T \mathbf{e} + w_u. \quad (12)$$

Here,  $s_u$  is the desired symbol at the  $u$ th user. Moreover,  $\mathbf{p}_u$  and  $\mathbf{p}_r$  denote the  $u$ th and the  $r$ th columns of the precoding matrix  $\mathbf{P}$ , respectively. The second, third and fourth terms in the right-hand side of (12) are the inter-user interference, the received nonlinear distortion, and the AWGN, respectively. The sum of these three terms can be considered as the effective noise and distortion. It should be noted that this effective noise is, in general, not Gaussian due to the PA nonlinearity. In order to obtain a lower bound on the sum rate, we rely on the fact that Gaussian noise is the worst-case additive noise (in terms of mutual information) for Gaussian inputs under a covariance constraint [27]. Accordingly, by assuming that the effective noise is Gaussian distributed, we can express an achievable sum rate for a deterministic channel (that is perfectly known by the users) as<sup>1</sup>

$$R_{\text{sum}}(\mathbf{P}) = \sum_{u=1}^U \log_2 (1 + \text{SINDR}_u(\mathbf{P})), \quad (13)$$

where

$$\text{SINDR}_u(\mathbf{P}) = \frac{|\mathbf{h}_u^T \mathbf{G}(\mathbf{P}) \mathbf{p}_u|^2}{\sum_{r \neq u} |\mathbf{h}_u^T \mathbf{G}(\mathbf{P}) \mathbf{p}_r|^2 + \mathbf{h}_u^T \mathbf{C}_e(\mathbf{P}) \mathbf{h}_u^* + N_0}, \quad (14)$$

is the signal-to-interference-noise and distortion ratio (SINDR) at the  $u$ th user.

### C. Precoding Matrix Normalization

We utilize the decomposition in (6) to introduce a procedure for precoding matrix normalization which is needed for controlling the average total transmit power under different choices of the precoding matrix. In particular, our objective is to find a real-valued normalization factor  $\alpha$  such that

$$\mathbb{E} [\|f(\alpha \mathbf{P} \mathbf{s})\|^2] = \rho_{\text{tot}}, \quad (15)$$

<sup>1</sup>The sum rate in (13) can be achieved by using a decoder that operates according to the nearest-neighbor principle, i.e., that returns the codeword that is closest to the received signal in the Euclidean norm.

where  $\rho_{\text{tot}}$  is a positive real value denoting the total power budget. This normalization can be formulated as the problem of finding the scalar  $\alpha$  such that  $\mathbb{E}[\|f(\alpha \mathbf{P}\mathbf{s})\|^2] = \rho_{\text{tot}}$ . Let us define  $\mathbf{z} = f(\alpha \mathbf{P}\mathbf{s})$  and  $\mathbf{C}_z = \mathbb{E}[\mathbf{z}\mathbf{z}^H]$ . Then, the normalization problem can be rewritten as finding  $\alpha$  such that  $\text{tr}(\mathbf{C}_z) - \rho_{\text{tot}} = 0$ , i.e., via solving

$$\text{tr}(|\alpha|^2 \mathbf{G}\mathbf{P}\mathbf{P}^H\mathbf{G}^H + \mathbf{C}_e) - \rho_{\text{tot}} = 0, \quad (16)$$

where  $\mathbf{G}$  and  $\mathbf{C}_e$  are the Bussgang gain and covariance matrix of distortion corresponding to decomposition of  $f(\alpha \mathbf{P}\mathbf{s})$  as in (6). Using (7)–(9) and (10)–(11), we can express (16) as

$$\text{tr}\left(\sum_{k=0}^K |\alpha|^{2(k+1)} \mathbf{L}_k \mathbf{C}_x \odot |\mathbf{C}_x|^{2k} \mathbf{L}_k^H\right) - \rho_{\text{tot}} = 0. \quad (17)$$

We solve (17) for  $|\alpha|^2$  and then pick the positive real solution which yields the desired scalar  $\alpha$ .

#### IV. SPATIAL DIRECTION OF TRANSMITTED DISTORTION

In this section, we analyze the directivity of the nonlinear distortion term  $\mathbf{e}$  for different choices of the precoding matrix  $\mathbf{P}$ . To do so, we focus our attention to line-of-sight (LoS) channels. Let us assume that the transmit antennas in the system model depicted in Fig. 1 are arranged in a uniform linear array (ULA) with  $\lambda_c/2$  spacing (where  $\lambda_c$  is the carrier wavelength). Consider a single-path LoS channel between the transmitter and the  $u$ th user with an angle of departure (AoD) of  $\psi_u$ . Then, the channel coefficients for the plane-wave model can be expressed as<sup>2</sup>

$$[\mathbf{h}(\psi_u)]_b = e^{-j\pi(b-1)\cos(\psi_u)}, \quad (18)$$

for  $b = 1, \dots, B$ .

##### A. Directivity of Distortion with MRT Precoding

In order to study the directivity of the useful signal and distortion, we calculate the power of the linear and distortion terms in different directions  $\psi \in [0, 2\pi)$ . In particular, for a given precoding matrix  $\mathbf{P}$ , we evaluate

$$\rho_{\text{lin}}(\psi) = \mathbf{h}^T(\psi) \mathbf{G}\mathbf{P}\mathbf{P}^H\mathbf{G}^H \mathbf{h}^*(\psi), \quad (19)$$

<sup>2</sup>In this section, for simplicity, we ignore path-loss effects.

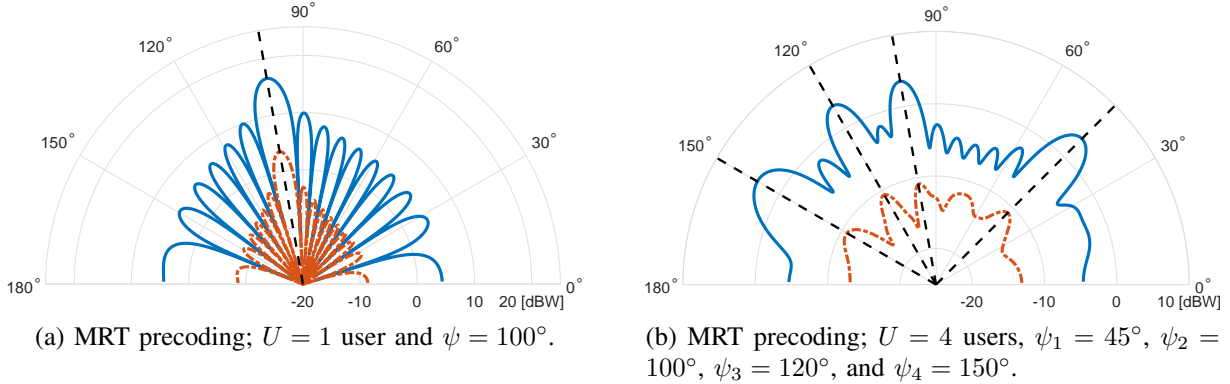


Fig. 2. Far-field radiation pattern for MRT precoding and equal PAs;  $B = 16$  antennas,  $U \in \{1, 4\}$  users. PA coefficients  $\beta_1^{(b)} = 0.98$  and  $\beta_3^{(b)} = -0.02 - 0.01j$  for  $b = 1, \dots, B$ . The precoding matrix is normalized such that the total transmit power is set to  $\rho_{\text{tot}} = 43$  dBm. The blue curves correspond to the radiated linear power  $\rho_{\text{lin}}(\psi)$  and the red curves correspond to the distortion power  $\rho_{\text{dist}}(\psi)$ . MRT precoding steers the distortion in the direction of user(s).

and

$$\rho_{\text{dist}}(\psi) = \mathbf{h}^T(\psi) \mathbf{C}_e \mathbf{h}^*(\psi), \quad (20)$$

which correspond to the radiated linear power and the distortion power, respectively. For the sake of simplicity, throughout this section, we consider only a third-order nonlinearity, namely,  $K = 1$  in (2), for which the Bussgang gain in (7)–(9) and the distortion covariance matrix in (10)–(11) reduce to [20]

$$\mathbf{G} = \mathbf{A}_1 \mathbf{I}_B + 2 \mathbf{A}_3 \text{diag}(\mathbf{P} \mathbf{P}^H), \quad (21)$$

and

$$\mathbf{C}_e(\mathbf{P}) = 2 \mathbf{A}_3 (\mathbf{P} \mathbf{P}^H \odot |\mathbf{P} \mathbf{P}^H|^2) \mathbf{A}_3^*, \quad (22)$$

respectively. Let us first consider the special case with  $U = 1$  user and equal PAs at different antennas. In this case, MRT precoder is given by  $\mathbf{p} = \alpha \mathbf{h}^* / \|\mathbf{h}\|$  where  $\alpha$  is the normalization factor that has been described in Section III-C. With this precoding in single-user scenarios, we get  $\mathbf{p} \mathbf{p}^H \odot |\mathbf{p} \mathbf{p}^H|^2 = c \mathbf{p} \mathbf{p}^H$  where  $c$  is a real scalar. As a result, by replacing (21) and (22) in (19) and (20), respectively, the directivity of the distortion matches exactly that of the linear term. This is illustrated in Fig. 2a, where we have plotted the far-field radiation pattern for MRT precoding in a setup with  $U = 1$  user and  $B = 16$  antennas with equal PAs,  $\beta_1^{(b)} = 0.98$  and  $\beta_3^{(b)} = -0.02 - 0.01j$  for  $b = 1, \dots, B$ .

Similarly, by evaluating (19) and (20) for MRT precoding in multiuser scenarios, i.e.,  $U > 1$ , where  $\mathbf{p}_u = \alpha \mathbf{h}_u^* / \|\mathbf{h}_u\|$  for  $u = 1, \dots, U$ , we can see that this precoding technique steers the

nonlinear distortion in the direction of the users. This phenomenon has been demonstrated for an example with  $U = 4$  in Fig. 2b.

The above analysis reveal that in presence of nonlinear PAs, MRT precoding can lead to a considerable performance degradation due to the beamforming of distortion<sup>3</sup>. Motivated by this, in what follows, we seek precoder design approaches that additionally take into account the directivity of distortion. In Section IV-B, we focus on a case with with possibly different PAs at different antennas and demonstrate that for single-user scenarios, properly designed precoders can fully eliminate the distortion in the direction of the user at the price of a reduced array gain. We refer to these precoders as zero-distortion precoders. Later on in Section V, we study precoder design in a general scenario with multiple users and arbitrary channel models.

### B. Zero-Distortion Precoding in Single-User Scenarios

We start by considering a simple scenario with a single user, i.e.,  $U = 1$ , and  $B = 2$  transmit antennas. To reduce complexity further, let us consider a third-order nonlinearity model with  $\beta_1^{(1)} = \beta_1^{(2)} = 1$ . In absence of AWGN, we can write the received signal as

$$\begin{aligned} y &= \begin{bmatrix} h_1 & h_2 \end{bmatrix} \begin{bmatrix} p_1 s + \beta_3^{(1)} p_1 s |p_1 s|^2 \\ p_2 s + \beta_3^{(2)} p_2 s |p_2 s|^2 \end{bmatrix} \\ &= (h_1 p_1 + h_2 p_2) s + (\beta_3^{(1)} h_1 p_1 |p_1|^2 + \beta_3^{(2)} h_2 p_2 |p_2|^2) s |s|^2, \end{aligned} \quad (23)$$

where  $p_1$  and  $p_2$  are the precoding coefficients associated with the first and the second antenna at the base station, respectively. It follows from (23) that, to have zero distortion at the UE, the precoding coefficients must satisfy

$$\beta_3^{(1)} h_1 p_1 |p_1|^2 + \beta_3^{(2)} h_2 p_2 |p_2|^2 = 0. \quad (24)$$

For the LoS channel given in (18) with a single user at angle  $\psi$ , the following precoder is a solution for (24)<sup>4</sup>:

$$\mathbf{p} = \alpha \begin{bmatrix} 1 \\ \left| \frac{\beta_3^{(1)}}{\beta_3^{(2)}} \right|^{\frac{1}{3}} e^{j(\pi \cos(\psi) + \pi + \angle \frac{\beta_3^{(1)}}{\beta_3^{(2)}})} \end{bmatrix}, \quad (25)$$

<sup>3</sup>The same statement is true for ZF precoding.

<sup>4</sup>This solution can also be found by setting  $\rho_{\text{dist}}(\psi)$  to zero.

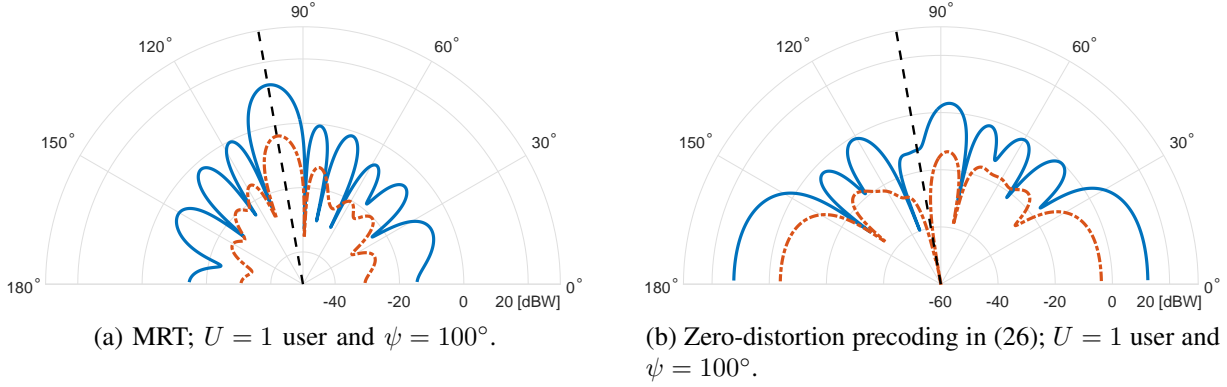


Fig. 3. Far-field radiation pattern for MRT and zero-distortion precoding with unequal PAs;  $B = 10$  antennas and  $U = 1$  user at  $\psi = 100^\circ$ . Total transmit power is set to  $\rho_{\text{tot}} = 43$  dBm. The nonlinearity coefficients are as in Table I. The blue curve corresponds to the linear term of the transmitted signal and the red curve corresponds to the distortion term. Zero-distortion precoder nulls the distortion in the direction of the user while reducing array gain by about 25 dB compared to MRT.

where  $\alpha$  is the normalization factor (as described in Section III-C). Note that if  $\beta_3^{(1)} = \beta_3^{(2)}$ , namely, when the PAs at two antenna ports are identical, the received useful (linear) signal is also zero. So, no useful signal is received by the user. Therefore, in order for this precoder to yield positive achievable rates over a LoS channel, PAs with different distortion profiles are needed at different antenna ports.

For  $B > 2$ , the problem becomes under-determined and various precoders may be found that result in zero distortion. For example, when  $B$  is odd, the following precoder yields zero distortion:

$$\mathbf{p} = \alpha \begin{bmatrix} 1 \\ \left| \frac{\beta_3^{(1)}}{\beta_3^{(2)}} \right|^{\frac{1}{3}} e^{j(\pi \cos(\psi) + \pi + \angle \frac{\beta_3^{(1)}}{\beta_3^{(2)}})} \\ 1 \\ \left| \frac{\beta_3^{(3)}}{\beta_3^{(4)}} \right|^{\frac{1}{3}} e^{j(\pi \cos(\psi) + \pi + \angle \frac{\beta_3^{(3)}}{\beta_3^{(4)}})} \\ \vdots \\ 1 \\ \left| \frac{\beta_3^{(B-1)}}{\beta_3^{(B)}} \right|^{\frac{1}{3}} e^{j(\pi \cos(\psi) + \pi + \angle \frac{\beta_3^{(B-1)}}{\beta_3^{(B)}})} \end{bmatrix}. \quad (26)$$

Fig. 3 depicts the far-field radiation pattern for MRT as well as the zero-distortion precoding given in (26) for a setup with a single user and  $B = 10$  antennas with different PAs at different antenna ports. The nonlinearity parameters for the PAs are given in Table I. It can be seen from Fig. 3b that the zero-distortion precoder nulls the distortion in the direction of the user at the

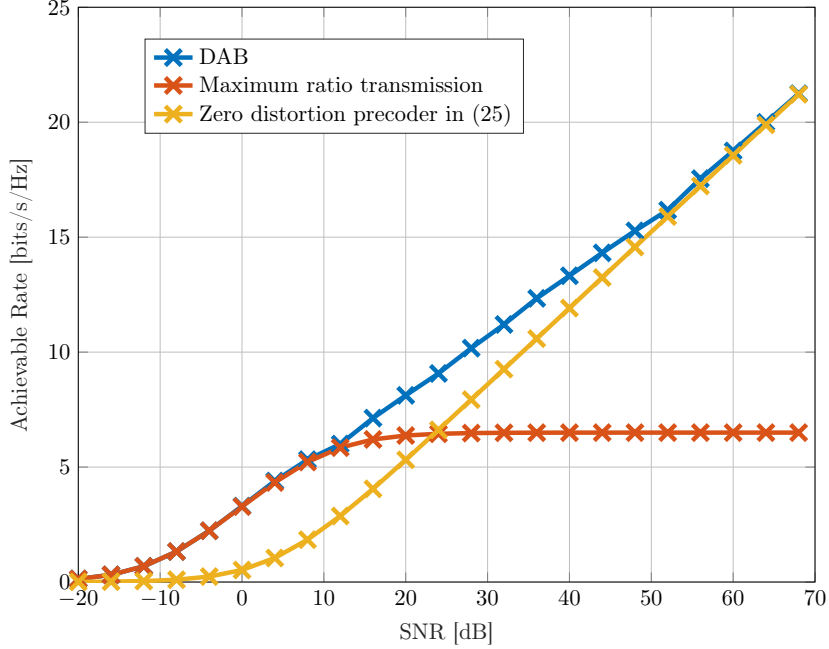


Fig. 4. Achievable rates averaged over 500 realizations of LoS channels in (18) with uniformly randomly distributed AoDs  $\psi \in [0, 180)$ ,  $B = 10$  antennas at base station and  $U = 1$  user. The nonlinearity coefficients are as in Table I. With distortion-aware precoding, the achievable rate becomes a strictly increasing function of SNR.

price of a considerably reduced array gain (about 25 dB reduction compared to that of MRT precoding as depicted in Fig. 3a).

In Fig. 4, for different SNR values, where we define  $\text{SNR} = \rho_{\text{tot}}/N_0$ , we evaluate the sum rate values in (13) for the precoder in (26) as well as the MRT precoding over LoS channels with  $B = 10$  and  $U = 1$ . It can be seen that the MRT precoder can achieve a higher rate than the zero-distortion precoder at low SNR values where AWGN dominates the nonlinear distortion. However, at higher SNRs, where the nonlinear distortion is dominant, the achievable rate for MRT saturates, whereas the achievable rate for the precoder in (26) is a strictly increasing function of SNR.

TABLE I  
PA NONLINEARITY PARAMETERS IN THE EXAMPLES DEMONSTRATED IN FIGS 3, 4 AND 5.

$\beta_1^{(1)}$	$\beta_1^{(2)}$	$\beta_1^{(3)}$	$\beta_1^{(4)}$	$\beta_1^{(5)}$	$\beta_1^{(6)}$	$\beta_1^{(7)}$	$\beta_1^{(8)}$	$\beta_1^{(9)}$	$\beta_1^{(10)}$
1.047	1.026	1.021	1.027	1.003	1.040	1.000	1.011	1.038	1.029
$\beta_3^{(1)}$	$\beta_3^{(2)}$	$\beta_3^{(3)}$	$\beta_3^{(4)}$	$\beta_3^{(5)}$	$\beta_3^{(6)}$	$\beta_3^{(7)}$	$\beta_3^{(8)}$	$\beta_3^{(9)}$	$\beta_3^{(10)}$
-0.024	-0.032	0.043	-0.03	-0.022	-0.018	-0.051	-0.042	-0.042	-0.030
-0.015j	-0.015j	-0.013j	-0.014j	-0.028j	-0.018j	-0.010j	-0.021j	-0.021j	-0.019j

As a "sneak peek" of what we are going to describe in the next section, we have also included the results achieved by DAB precoding scheme which achieves an enhanced performance over the whole range of SNR and converges to the zero-distortion precoder at high SNR values. The algorithm explained in the next section is based on a general precoder design framework that is able to simultaneously take into account the effect of the linear precoder on the array gain, the distortion, and the multiuser interference.

## V. DISTORTION-AWARE PRECODING

In this section, we formulate the distortion-aware precoder design problem as a non-convex optimization problem with the objective of optimizing the linear precoder such that the lower bound on the sum rate in (13) is maximized. We introduce an iterative algorithm to solve this problem approximately using gradient ascent.

### A. Distortion-Aware Beamforming (DAB)

The choice of the precoding matrix  $\mathbf{P}$  affects the sum rate as it controls the array gain, the multi-user interference, and the distortion radiated in the direction of the users (as we saw in Section IV). Under the assumption that the transmitter has perfect CSI as well as knowledge of the PA nonlinearity parameters, our objective is to find the precoding matrix  $\mathbf{P}$  that maximizes the sum rate in (13) under an equality constraint on the average total transmit power. This optimization problem can be formulated as follows:

$$\begin{aligned} & \underset{\mathbf{P} \in \mathbb{C}^{B \times U}}{\text{maximize}} \quad R_{\text{sum}}(\mathbf{P}) \\ & \text{subject to} \quad \mathbb{E}[\|f(\mathbf{Ps})\|^2] = \rho_{\text{tot}}, \end{aligned} \tag{27}$$

where  $R_{\text{sum}}(\mathbf{P})$  is defined in (13) and  $\rho_{\text{tot}}$  denotes the average total transmit power. Note that (27) is a non-convex optimization problem since  $R_{\text{sum}}(\mathbf{P})$  is a non-convex function of  $\mathbf{P}$ . Inspired by the solution in [28, Section V], in what follows, we solve this problem approximately using an iterative projected gradient ascent algorithm. We refer to this algorithm as DAB.

In particular, DAB updates the precoding matrix by taking steps along the steepest ascent direction of the objective function  $R_{\text{sum}}(\mathbf{P})$ . The resulting precoding matrix is then normalized to ensure the feasibility of the solution. This procedure can be formulated as [28, Eq. (72)]

$$\tilde{\mathbf{P}} = [\mathbf{P}^{(i-1)} + \mu^{(i-1)} \nabla_{\mathbf{P}} R_{\text{sum}}(\mathbf{P}^{(i-1)})]_{\mathbb{E}\|f(\mathbf{P}^{(i-1)}\mathbf{s})\|^2 = \rho_{\text{tot}}}^+. \tag{28}$$

Here,  $i = 1, \dots, I$  is the iteration index,  $I$  is the maximum number of iterations,  $\mu^{(i)}$  is the step size of the  $i$ th iteration, and  $[\cdot]^+_{\mathbb{E}\|f(\mathbf{P}^{(i-1)}\mathbf{s})\|^2 = \rho_{\text{tot}}}$  denotes normalization of the updated precoding matrix such that the power constraint  $\mathbb{E}\left[\|f(\mathbf{P}^{(i-1)}\mathbf{s})\|^2\right] = \rho_{\text{tot}}$  is satisfied. The details of this normalization has been explained in Section III-C. If  $R_{\text{sum}}(\tilde{\mathbf{P}}) > R_{\text{sum}}(\mathbf{P}^{(i-1)})$ , we update the precoding matrix to  $\mathbf{P}^{(i)} = \tilde{\mathbf{P}}$  and reset the step size  $\mu^{(i)} = \mu^{(0)}$ . Otherwise, we do not update the precoding matrix, i.e.,  $\mathbf{P}^{(i)} = \mathbf{P}^{(i-1)}$ , and decrease the step size  $\mu^{(i)} = \frac{1}{2}\mu^{(i-1)}$ . Finally, we choose  $\mathbf{P}_{\text{DAB}} = \mathbf{P}^{(I)}$  as the output of the algorithm. We refer to this solution as the DAB precoding matrix. In Algorithm 1, we summarize the steps required for computing the DAB precoding matrix using the projected gradient ascent approach.

We now explain the procedure for gradient calculation in (28). The gradient calculation can be carried out either numerically or through evaluation of the closed-form expression. In order to compute  $\nabla_{\mathbf{P}} R_{\text{sum}}(\mathbf{P})$  numerically, we shall evaluate

$$[\nabla_{\mathbf{P}} R_{\text{sum}}(\mathbf{P})]_{b,u} \approx \frac{\left(R_{\text{sum}}(\mathbf{P} + \Delta_r^{(b,u)}) - R_{\text{sum}}(\mathbf{P})\right) + j\left(R_{\text{sum}}(\mathbf{P} + \Delta_i^{(b,u)}) - R_{\text{sum}}(\mathbf{P})\right)}{\delta}, \quad (29)$$

for  $b = 1, \dots, B$  and  $u = 1, \dots, U$ , where  $\delta$  is a small positive constant and  $\Delta_r^{(b,u)}$  is a  $B \times U$  matrix with  $\delta$  at the  $b$ th row and the  $u$ th column and zero entries at all other positions. Similarly,  $\Delta_i^{(b,u)}$  is a  $B \times U$  matrix whose only non-zero entry is  $j\delta$  at the  $b$ th row and the  $u$ th column. A more accurate way of calculating this gradient is via deriving and evaluating closed-form expressions; this has been addressed for the special case of third-order nonlinearity ( $K = 1$ ) in Appendix A.

Due to the non-convexity of the problem, Algorithm 1 does not provide global optimality guarantees, i.e., it can return a local maximum. In order to increase the likelihood of Algorithm 1 to converge to the global maximum, we repeat it with multiple initializations and pick the solution that achieves the highest sum rate. Including the conventional precoding matrices, i.e., MRT and ZF, among the set of initializations can help accelerating the convergence and it guarantees that the DAB precoder does not perform worse than these precoders.

## VI. ENERGY-EFFICIENT DISTORTION-AWARE PRECODING

In Section V, we studied the precoder design with the objective of maximizing the sum rate under a given power constraint. The average total power constraint in (27) does not take into account the maximum output power constraint of the individual PAs. In this section, we consider

---

**Algorithm 1** Algorithm for computing the distortion-aware beamforming (DAB) precoding matrix.

---

**Inputs:**  $\mathbf{h}_1, \dots, \mathbf{h}_U, \beta_1^{(b)}, \dots, \beta_K^{(b)}$  for  $b = 1, \dots, B$ ,  $\rho_{\text{tot}}$ , and  $N_0$

**Output:**  $\mathbf{P}_{\text{DAB}}$

*Initialization:*  $\mu^{(0)}$  and  $\mathbf{P}^{(0)}$

- 1:  $R_{\text{sum}}^{(0)} \leftarrow R_{\text{sum}}(\mathbf{P}^{(0)})$
- 2: **for**  $i = 1, \dots, I$  **do**
- 3:    $\tilde{\mathbf{P}} \leftarrow [\mathbf{P}^{(i-1)} + \mu^{(i-1)} \nabla_{\mathbf{P}} R_{\text{sum}}(\mathbf{P}^{(i-1)})]_{\mathbb{E} \|f(\mathbf{P}^{(i-1)} \mathbf{s})\|^2 = \rho_{\text{tot}}}^+$
- 4:    $\tilde{R}_{\text{sum}} \leftarrow R_{\text{sum}}(\tilde{\mathbf{P}})$
- 5:   **if**  $\tilde{R}_{\text{sum}} > R_{\text{sum}}^{(i-1)}$  **then**
- 6:      $\mathbf{P}^{(i)} \leftarrow \tilde{\mathbf{P}}, R_{\text{sum}}^{(i)} \leftarrow \tilde{R}_{\text{sum}}$ , and  $\mu^{(i)} \leftarrow \mu^{(0)}$
- 7:   **else**
- 8:      $\mathbf{P}^{(i)} \leftarrow \mathbf{P}^{(i-1)}, R_{\text{sum}}^{(i)} \leftarrow R_{\text{sum}}^{(i-1)}$ , and  $\mu^{(i)} \leftarrow \frac{1}{2} \mu^{(i-1)}$
- 9:   **end if**
- 10: **end for**
- 11:  $\mathbf{P}_{\text{DAB}} \leftarrow \mathbf{P}^{(I)}$

---

a precoding matrix optimization problem, in which the precoding matrix is subjected to a per-antenna maximum radiated power constraint. Furthermore, we adopt the model in [25] to quantify the total base station side consumed power. This model takes into account the dissipated power in addition to the sum radiated power which allows for evaluation and optimization of energy efficiency.

A common way for quantifying energy efficiency is via the evaluation of the ratio between throughput and consumed power [29]

$$\eta_{\text{EE}} = \frac{W R_{\text{sum}}(\mathbf{P})}{\rho_{\text{cons,tot}}(\mathbf{P})}, \quad (30)$$

measured in bits per Joule. Here,  $W$  denotes the bandwidth and  $\rho_{\text{cons,tot}}(\mathbf{P}) = \sum_{b=1}^B \rho_{\text{cons},b}(\mathbf{P})$  is the total consumed power which can be evaluated using (5). In an attempt to maximize energy efficiency, we seek the precoding matrix  $\mathbf{P}$  that minimizes the consumed power while guaranteeing a given minimum required sum rate, i.e.,

$$R_{\text{sum}}(\mathbf{P}) \geq R_0, \quad (31)$$

and under a per-antenna power constraint given by

$$\rho_{tx,b} = \mathbb{E}[|f_b(x_b)|^2] \leq \rho_{\max,b}, \quad (32)$$

for  $b = 1, \dots, B$ . In (32),  $x_b$  is the precoded signal input to the  $b$ th PA and can be obtained by multiplying the  $b$ th row of the precoding matrix  $\mathbf{P}$  by the transmitted symbols  $\mathbf{s}$ . The energy efficiency maximization problem can be formulated as

$$\begin{aligned} & \underset{\mathbf{P} \in \mathbb{C}^{B \times U}}{\text{minimize}} \quad \rho_{\text{cons,tot}}(\mathbf{P}) \\ & \text{subject to} \quad (31) \text{ and (32).} \end{aligned} \quad (33)$$

We solve the non-convex problem in (33) approximately in two steps. First, we find the precoding matrix that maximizes the sum rate under a per-antenna power constraint, namely, we maximize  $R_{\text{sum}}(\mathbf{P})$  subject to (32). We refer to this problem as **S1**. Then, starting from the solution of **S1**, we minimize the consumed power by updating the precoding matrix along the descent direction of the consumed power  $\rho_{\text{cons,tot}}(\mathbf{P})$  until (31) is violated or a maximum number of iterations is reached. This problem is referred to as **S2** and its output, which is an approximate solution of (33)–(31), is called energy-efficient DAB (EE-DAB) precoding matrix.

With a slight modification, Algorithm 1 in Section V can be used to solve **S1**. In particular, by replacing (28) (step 3 in Algorithm 1) with

$$\tilde{\mathbf{P}} = [\mathbf{P}^{(i-1)} + \mu^{(i-1)} \nabla_{\mathbf{P}} R_{\text{sum}}(\mathbf{P}^{(i-1)})]_{\mathbb{E}[|f_b(x_b)|^2] \leq \rho_{\max,b}}^+, \quad (34)$$

where  $[\cdot]_{\mathbb{E}[|f_b(x_b)|^2] \leq \rho_{\max,b}}^+$  denotes *occasional* normalization of the  $b$ th row of the precoding matrix  $\mathbf{P}$  such that (32) is satisfied. This is to say, after updating the precoding matrix (on line 3 of Algorithm 1), normalization is carried out only if the per-antenna power constraint is violated at one or more antennas. For these antennas, the normalization problem is equivalent to finding the values of the scalars  $\alpha_{\hat{b}}$  such that  $\mathbb{E}[|f(\alpha_{\hat{b}} x_{\hat{b}})|^2] = \rho_{\max,\hat{b}}$  where  $\hat{b}$  denotes the index of an antenna for which (32) is violated. The normalization problem can be solved using the same procedure described in (16)–(17). Other than the normalization, all other steps of Algorithm 1 are implemented in the exact same way as explained in Section V.

Once **S1** is solved, its solution  $\mathbf{P}^{(\text{S1})}$  is used to initialize the algorithm for solving **S2**. This algorithm seeks the precoding matrix that minimizes the consumed power for a given sum rate no smaller than  $R_0$ . Specifically, it updates the precoding matrix using projected gradient descent

---

**Algorithm 2** Algorithm for computing the energy-efficient DAB (EE-DAB) precoding matrix.

---

**Inputs:**  $R_0, \mathbf{h}_1, \dots, \mathbf{h}_U, \beta_1^{(b)}, \dots, \beta_K^{(b)}, \rho_{\max,b}, \eta_{\max,b}$  for  $b = 1, \dots, B$ , and  $N_0$ 
**Output:**  $\mathbf{P}_{\text{EE-DAB}}$ 
*Initialization:*  $\mu^{(0)}$  and  $\mathbf{P}^{(S1)}$  from Algorithm 1 (with per-antenna normalization)

```

1:  $\rho_{\text{cons,tot}}^{(0)} \leftarrow \rho_{\text{cons,tot}}(\mathbf{P}^{(S1)})$  and  $i = 1$ 
2: while  $R_{\text{sum}}(\mathbf{P}^{(i)}) \geq R_0$  and  $i \leq I$  do
3:    $\tilde{\mathbf{P}} \leftarrow [\mathbf{P}^{(i-1)} - \mu^{(i-1)} \nabla_{\mathbf{P}} \rho_{\text{cons,tot}}(\mathbf{P}^{(i-1)})]_{\mathbb{E}[\|f_b(x_b)\|^2] \leq \rho_{\max,b}}^+$ 
4:    $\tilde{\rho}_{\text{cons,tot}} \leftarrow \rho_{\text{cons,tot}}(\tilde{\mathbf{P}})$ 
5:   if  $\tilde{\rho}_{\text{cons,tot}} < \rho_{\text{cons,tot}}^{(i-1)}$  then
6:      $\mathbf{P}^{(i)} \leftarrow \tilde{\mathbf{P}}, \rho_{\text{cons,tot}}^{(i)} \leftarrow \tilde{\rho}_{\text{cons,tot}}$ , and  $\mu^{(i)} \leftarrow \mu^{(0)}$ 
7:   else
8:      $\mathbf{P}^{(i)} \leftarrow \mathbf{P}^{(i-1)}, \rho_{\text{cons,tot}}^{(i)} \leftarrow \rho_{\text{cons,tot}}^{(i-1)}$ , and  $\mu^{(i)} \leftarrow \frac{1}{2}\mu^{(i-1)}$ 
9:   end if
10:   $i = i + 1$ 
11: end while
12:  $\mathbf{P}_{\text{DAB}} \leftarrow \mathbf{P}^{(\hat{i})}$  where  $\hat{i} = i - 1$  is the final iteration where stopping criterion is met.

```

---

where in each iteration,

$$\tilde{\mathbf{P}} = [\mathbf{P}^{(i-1)} - \mu^{(i-1)} \nabla_{\mathbf{P}} \rho_{\text{cons,tot}}(\mathbf{P}^{(i-1)})]_{\mathbb{E}[\|f_b(x_b)\|^2] \leq \rho_{\max,b}}^+, \quad (35)$$

for  $i = 1, \dots, I$  where  $\mathbf{P}^{(0)} = \mathbf{P}^{(S1)}$ . The gradient  $\nabla_{\mathbf{P}} \rho_{\text{cons,tot}}(\mathbf{P}^{(i-1)})$  can be evaluated, similarly to (29), as

$$\begin{aligned} & [\nabla_{\mathbf{P}} \rho_{\text{cons,tot}}(\mathbf{P})]_{b,u} \\ & \approx \frac{(\rho_{\text{cons,tot}}(\mathbf{P} + \Delta_r^{(b,u)}) - \rho_{\text{cons,tot}}(\mathbf{P})) + j(\rho_{\text{cons,tot}}(\mathbf{P} + \Delta_i^{(b,u)}) - \rho_{\text{cons,tot}}(\mathbf{P}))}{\delta}, \end{aligned} \quad (36)$$

for  $b = 1, \dots, B$  and  $u = 1, \dots, U$ . The normalization in (35), similarly to that of (34), is carried out occasionally and on the rows of the precoding matrix that violate (32). At each iteration, if  $\rho_{\text{cons,tot}}(\tilde{\mathbf{P}}) < \rho_{\text{cons,tot}}(\mathbf{P}^{(i-1)})$ , the precoding matrix is updated to  $\mathbf{P}^{(i)} = \tilde{\mathbf{P}}$  and the step size is reset to  $\mu^{(i)} = \mu^{(0)}$ . Otherwise, the step size is decreased according to  $\mu^{(i)} = \frac{1}{2}\mu^{(i-1)}$ . This procedure is repeated until either the sum rate goes below  $R_0$  or the maximum number of iteration  $I$ , is reached. This procedure is summarized in Algorithm 2. Since the consumed power does not increase across iterations and since it is bounded from below (non-negative), the convergence of this algorithm is guaranteed.

## VII. NUMERICAL RESULTS

We verify the efficacy of the proposed framework by means of numerical simulations. We first describe the channel model that we use for our simulations (except for the example in Section VII-E). We then compare the spectral and energy efficiencies achieved by DAB and EE-DAB with those achieved by MRT and ZF precoding. Finally, we evaluate the out-of-band radiation associated to the proposed precoding techniques.

### A. Geometric Channel Model

In what follows, unless otherwise stated, we adopt a channel model that captures the sparse scattering characteristics of millimeter-wave channels in non-LoS (nLoS) environments, namely, when there is no dominant path. In this model, which is typically referred to as geometric channel model, each scatterer contributes to a single path and the channel coefficients can be expressed as [30], [31]

$$\mathbf{h}_u = \sqrt{\frac{B}{N_{\text{path}}}} \sum_{\ell=1}^{N_{\text{path}}} \zeta_{u,\ell} \mathbf{a}(\psi_{u,\ell}), \quad (37)$$

for  $u = 1, \dots, U$ , where  $N_{\text{path}}$  represents the number of paths/scatterers. Here,  $\zeta_{u,\ell} \sim \mathcal{CN}(0, \gamma^2)$  is the independent and identically distributed (i.i.d.) channel gain (including path loss) corresponding to the  $\ell$ th path. We assume that the path loss for all the users is equal to  $\gamma^2$ . Furthermore,  $\psi_{u,\ell}$  is the AoD for the  $\ell$ th path, and  $\mathbf{a}(\psi_{u,\ell})$  is the corresponding array response vector. For a ULA with  $\lambda_c/2$  antenna spacing, the  $b$ th entry of  $\mathbf{a}(\psi_{u,\ell})$  is given by

$$[\mathbf{a}(\psi_{u,\ell})]_b = \frac{1}{\sqrt{B}} e^{-j\pi(b-1)\cos(\psi_{u,\ell})}, \quad (38)$$

for  $b = 1, \dots, B$ . We use the following SNR definition:

$$\text{SNR} = \gamma^2 \frac{\rho_{\text{tot}}}{N_0}. \quad (39)$$

### B. Spectral Efficiency: DAB versus Conventional Precoders

We compare the spectral efficiency of Algorithm 1, namely DAB, with those of conventional precoding techniques including ZF and MRT. To this end, we characterize the statistics of the achievable sum rate in (13) by considering  $10^3$  random realizations of the model in (37) with  $N_{\text{path}} = 4$  and under the assumption that the AoD  $\psi_{u,\ell}$  is uniformly distributed over the interval

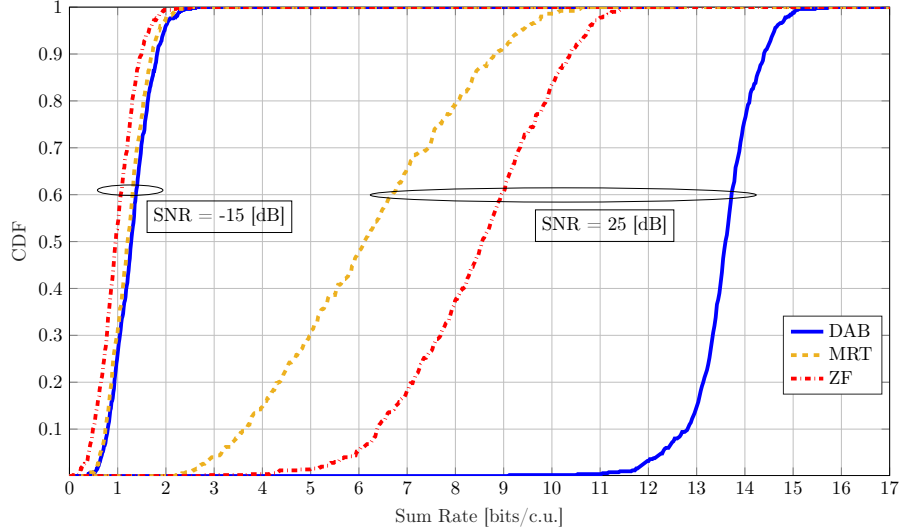


Fig. 5. CDF of sum rates with different linear precoders; geometric channel model with  $N_{\text{path}} = 4$  and AoDs  $\psi_{u,\ell}$  uniformly distributed over  $[0^\circ, 180^\circ]$ ,  $B = 10$  antennas,  $U = 2$  users, nonlinearity parameters as given in Table I,  $\rho_{\text{tot}} = 43$  dBm, and  $\text{SNR} \in \{-15, 25\}$  dB.

$[0^\circ, 180^\circ]$ ). By adopting the nLoS path-loss model presented in [32, Table I] and by assuming that the system operates at a carrier frequency  $f_c = 28$  GHz (such that  $\lambda_c \approx 10.7$  mm) with the average distance from the transmitter to the users being 20 m, we find that the average path loss is  $\gamma^2 = -110$  dB.

In Fig. 5, the cumulative distribution function (CDF) of achievable sum rate is plotted for DAB, ZF, and MRT. In this example,  $B = 10$  antennas and  $U = 2$  users are considered. The nonlinearity characteristics of the PAs at different transmit antennas are as given in Table I. The total transmit power is set to  $\rho_{\text{tot}} = 43$  dBm and the CDF is plotted for two SNR values, namely  $-15$  and  $25$  dB. We see that the DAB precoding technique outperforms the conventional linear precoders that do not take into account the distortion introduced by the nonlinear PAs. The improvement in performance is more evident at high SNR values. This is because, at low SNR (i.e.,  $\text{SNR} = -15$  dB), the thermal noise dominates the nonlinear distortion. As a result, dealing with distortion is not necessary and the DAB precoder converges to the MRT precoder (as was also shown in Fig. 4). In the high-SNR regime, however, the performance of both MRT and ZF is limited by the nonlinear distortion. As a result, DAB provides considerable gains over these two conventional precoding techniques.

In Fig. 6, we illustrate the performance gains achieved by DAB over ZF at  $\text{SNR} = 25$  dB,

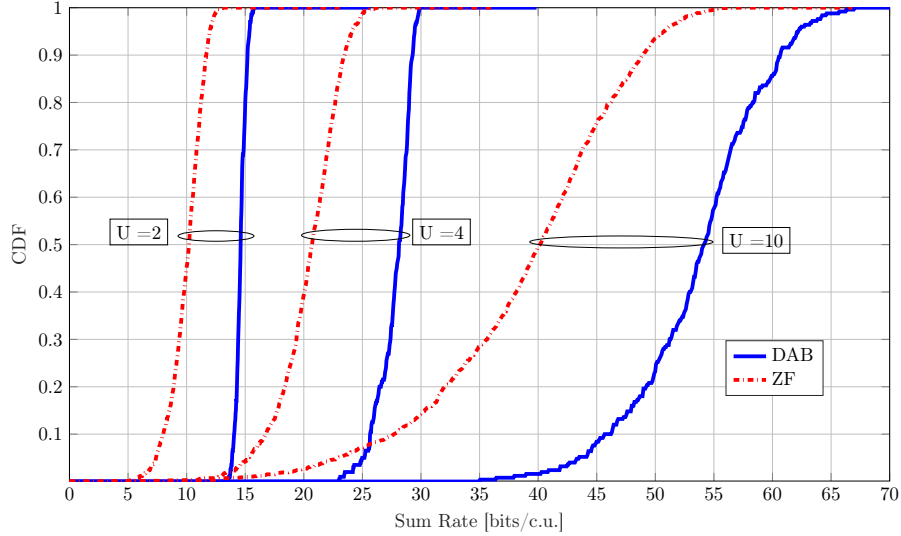


Fig. 6. CDF of the sum rate with ZF and DAB precoders with different number of users  $U \in \{2, 4, 10\}$ ; geometric channel model with  $N_{\text{path}} = 4$  and  $\gamma^2 = -110$  dB, AoDs  $\psi_{u,\ell}$  uniformly distributed over  $[0^\circ, 180^\circ]$ ,  $B = 16$  antennas, equal PAs with  $\beta_1^{(b)} = 0.98$ ,  $\beta_3^{(b)} = -0.04 - 0.01j$  and  $\beta_5^{(b)} = -0.001 - 0.002j$  for  $b = 1, \dots, B$ ,  $\rho_{\text{tot}} = 43$  dBm, and SNR = 25 dB.

for a different number of users. Specifically, we consider  $B = 16$  antennas at the transmitter all equipped with equal PAs with  $\beta_1^{(b)} = 0.98$ ,  $\beta_3^{(b)} = -0.04 - 0.01j$ , and  $\beta_5^{(b)} = -0.001 - 0.002j$  for  $b = 1, \dots, B$ . We consider the same channel model as in Fig. 5 and characterize the CDF of the sum rate for  $U = 2, 4$ , and 10 users. Our results reveal that the relative performance gains attainable with DAB over ZF decreases as the number of users increase. For instance, while for  $U = 2$  users, DAB achieves roughly a 50% sum rate improvement over ZF at CDF equal to 0.5, this gain reduces to about 35% when  $U = 10$  at the same CDF level. This behavior is due to the fact that by increasing the number of users, distortion correlation becomes less significant and as a result, benefits of distortion-aware precoders become less pronounced. This is in line with the observations made in the studies that considered distortion-aware solutions for uplink massive MIMO systems (see, e.g., [21], [33], [34]).

### C. Energy Efficiency: EE-DAB versus ZF

In order to evaluate the energy efficiency of EE-DAB precoding, we plot the CDF of the consumed power  $\sum_{b=1}^B \rho_{\text{cons},b}$  for different minimum required sum rate,  $R_0$ , values. We consider a setup with  $B = 32$  and  $U = 4$ . The channel model and nonlinearity characteristics of the PAs are the same as in Fig. 6. The parameters associated with PA power consumption are set as

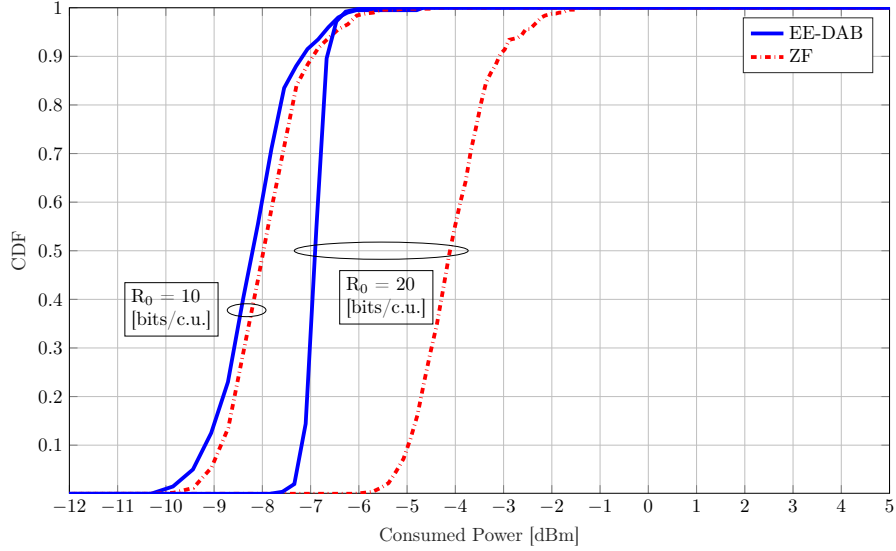


Fig. 7. CDF of total base station side consumed power with ZF and EE-DAB precoders for different  $R_0$  values; geometric channel model with  $N_{\text{path}} = 4$  and  $\gamma^2 = -110$  dB, AoDs  $\psi_{u,\ell}$  uniformly distributed over  $[0^\circ, 180^\circ]$ ,  $U = 4$  users,  $B = 32$  antennas, equal PAs with  $\beta_1^{(b)} = 0.98$ ,  $\beta_3^{(b)} = -0.04 - 0.01j$  and  $\beta_5^{(b)} = -0.001 - 0.002j$  for  $b = 1, \dots, B$ , power consumption model parameters  $\eta_{\max,b} = 0.55$  and  $\rho_{\max,b} = 5$  dBm, and noise power  $N_0 = -70$  dBm.

$\eta_{\max,b} = 0.55$  and  $\rho_{\max,b} = 5$  dBm for all  $b = 1, \dots, B$ . The noise power is  $N_0 = -70$  dBm and the consumed-power values are calculated for the precoding matrices acquired via Algorithm 2 for  $R_0 \in \{10, 20\}$  bits per channel use (bits/c.u.). As a benchmark, we also evaluate the power consumption of the ZF precoder with a normalization such that  $R_0$  is achieved. The resulting CDF is given in Fig. 7.

It can be seen from Fig. 7 that, by taking the power consumption into account (in addition to the effect of nonlinear distortion), EE-DAB can achieve a given sum rate with a lower consumed power than ZF precoding. This improvement is achieved via optimizing the transmit power in addition to directivity of linear signal and distortion using Algorithm 2. EE-DAB's enhanced performance with respect to ZF is more evident at scenarios with higher rate requirements. For instance, in this particular example, EE-DAB consumes 3 dB less power compared to ZF in order to achieve  $R_0 = 20$  bits/c.u. at the CDF equal to 0.6. However, for achieving  $R_0 = 10$  bits/c.u., the consumed power for EE-DAB is only about 0.25 dB less than that of the ZF.

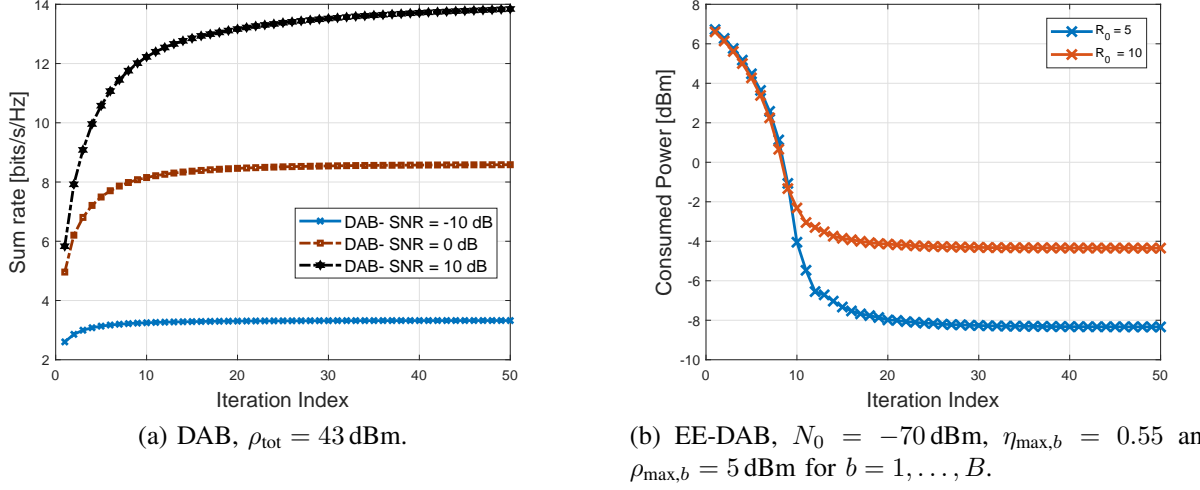


Fig. 8. Average convergence behavior of Algorithms 1 and 2; geometric channel model,  $N_{\text{path}} = 4$  paths and  $\gamma^2 = -110 \text{ dB}$ ,  $B = 16$  antennas,  $U = 2$  users,  $\beta_1^{(b)} = 0.98$ ,  $\beta_3^{(b)} = -0.04 - 0.01j$ ,  $\beta_5^{(b)} = -0.001 - 0.002j$  for  $b = 1, \dots, B$ . Both algorithms converge in a relatively low number of iterations.

#### D. Convergence of the Proposed Algorithms

The improved performance of the DAB and EE-DAB precoders compared to conventional linear precoders is achieved at the cost of increased computational complexity. Here, we study the convergence of Algorithms 1 and 2, which are used to obtain the DAB and EE-DAB precoders, respectively. This will provide insight into the number of iterations required for achieving a certain performance.

We consider a setup with  $B = 16$  and  $U = 2$ . The PA parameters are the same as in Figs 6 and 7. In Fig. 8a, we show the sum rate achieved by the DAB precoder as a function of the number of iterations. It can be seen that the convergence of Algorithm 1 is faster at low SNR compared to high SNR. Indeed, at low SNR, conventional precoding schemes are as good as DAB precoding (see Fig. 5). Therefore, since the MRT and ZF precoding matrices are included in the initialization, fast convergence is expected. At high SNR, however, the structure of the optimal precoder is significantly different from that of the MRT and ZF precoders which results in slower convergence. Fig. 8b depicts the convergence behavior of Algorithm 2. This demonstrates that both of the proposed algorithms converge in a relatively small number of iterations, keeping the computational complexity in a manageable range.

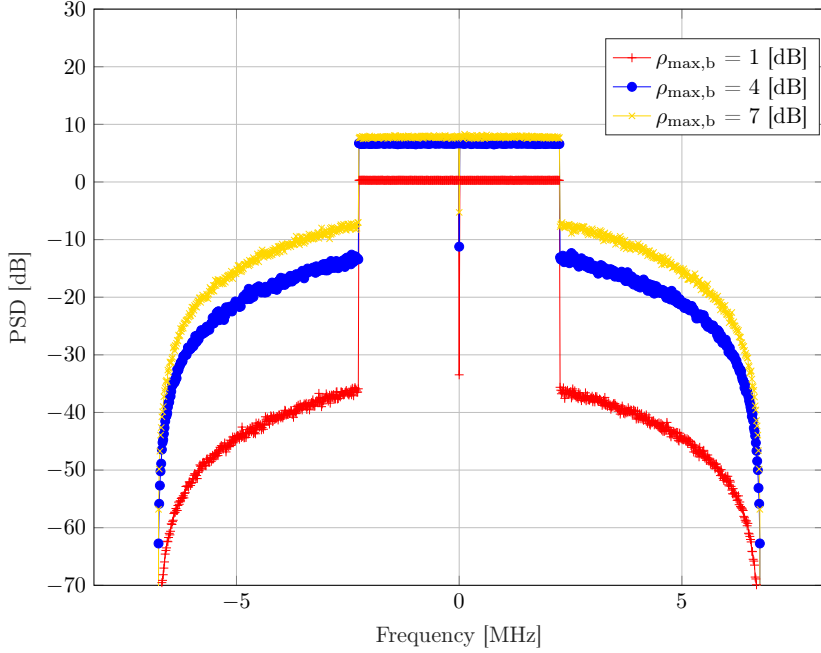


Fig. 9. PSD of transmitted signal from the antenna with the highest spectral regrowth with DAB under per-antenna power constraint in (32); LoS channel,  $B = 8$  antennas,  $U = 1$  user,  $\beta_1^{(b)} = 0.98$ ,  $\beta_3^{(b)} = -0.04 - 0.01j$  for  $b = 1, \dots, B$ . By controlling  $\rho_{\max,b}$ , we can bound the spectral regrowth within a given mask limit.

### E. Out-of-Band Emissions

In addition to analyses of the in-band distortion caused by the nonlinear PAs, which has been the main focus of this paper, analyses of out-of-band emissions are also of significant practical importance. With out-of-band emission, we refer to emissions at frequencies outside the allocated frequency band due to the PA nonlinearities. These emissions, which are undesirable because they interfere with concurrent transmission in adjacent bands, are strictly regulated in wireless standards.

We evaluate the spectral emissions with DAB precoding under a per-antenna power constraint (32) for different  $\rho_{\max,b}$  values. In Fig. 9, we plot the power spectral density (PSD) of the transmitted signal from the antenna with the highest spectral regrowth (worst case) in the array. We assume a LoS channel with  $B = 8$  and  $U = 1$ . Furthermore, we set the nonlinearity parameters to  $\beta_1^{(b)} = 0.98$  and  $\beta_3^{(b)} = -0.04 - 0.01j$  for  $b = 1, \dots, B$ . The precoding matrix is calculated using Algorithm 1 (while replacing step 3 with (34) to satisfy per-antenna transmit power constraints) and applied to an OFDM signal with a one-side bandwidth of 2.25 MHz. The total number of subcarriers is 1024, among which 300 subcarriers are occupied (the occupied

carriers are the first 150 to the left and to the right of the DC carrier). The results in Fig. 9 indicate that by controlling  $\rho_{\max,b}$ , one can limit spectral regrowth outside a given frequency band. It is indeed possible to generalize the proposed precoder optimization framework to account explicitly for OOB emission on top of in-band distortion. A detailed study of such more general framework is left for future works.

### VIII. CONCLUSIONS

We have shown that the choice of the precoding matrix has a direct impact on the amount and directivity of distortion emitted by nonlinear power amplifiers in the downlink of massive MIMO systems. Accordingly, we have introduced precoder optimization algorithms that incorporate the knowledge of the nonlinearity characteristic of the PAs as well as their power consumption. Through numerical examples, we have demonstrated that our proposed solutions can achieve considerable improvements in terms of spectral and energy efficiency with respect to conventional precoding techniques, i.e., zero-forcing and maximal ratio transmission. Moreover, by studying the out-of-band emission, we have shown that our proposed framework for precoder optimization can also be used for bounding the spectral regrowth due to nonlinear power amplifiers outside a given frequency band.

While the present study has primarily focused on the effect of distortion from nonlinear power amplifiers, the proposed algorithms can be generalized to account for the distortion caused by other hardware components, such as oscillators and low-resolution digital-to-analog converters. Starting from behavioral models of non-ideal hardware, one can find an equivalent input-output relationship, where the impaired signal is written as the sum of a useful signal plus an uncorrelated distortion (similar to (6)). By cascading these statistical models, it is possible to acquire an aggregate model for the combined effects of these impairments (see [19] for an example). The resulting Bussgang gain matrix and the covariance of Bussgang distortion term can be used within the precoder optimization framework (described in Algorithms 1 and 2), with the objective of compensating for the overall transmitter-side distortion.

APPENDIX A  
CLOSED-FORM EXPRESSION FOR  $\nabla_{\mathbf{P}} R_{\text{sum}}(\mathbf{P})$

We derive a closed-form expression for the gradient  $\nabla_{\mathbf{P}} R_{\text{sum}}(\mathbf{P})$ , which facilitates a more accurate evaluation of the update in (28) compared to its approximate numerical evaluation in (29). To this end, let

$$n_u(\mathbf{P}) = |\mathbf{h}_u^T \mathbf{G}(\mathbf{P}) \mathbf{p}_u|^2, \quad (40)$$

and

$$d_u(\mathbf{P}) = d_u^{\text{mui}}(\mathbf{P}) + d_u^{\text{dist}}(\mathbf{P}) + N_0, \quad (41)$$

denote the numerator and denominator of the SINDR in (14), respectively, where  $d_u^{\text{mui}}(\mathbf{P}) = \sum_{r \neq u} |\mathbf{h}_u^T \mathbf{G}(\mathbf{P}) \mathbf{p}_r|^2$  and  $d_u^{\text{dist}}(\mathbf{P}) = \mathbf{h}_u^T \mathbf{C}_e(\mathbf{P}) \mathbf{h}_u^*$  is the part of the denominator corresponding to multiuser interference and nonlinear distortion, respectively. With these definitions, the gradient  $\nabla_{\mathbf{P}} R_{\text{sum}}(\mathbf{P})$  can be written as

$$\nabla_{\mathbf{P}} R_{\text{sum}}(\mathbf{P}) = \sum_{u=1}^U \frac{2 \log_2(e)}{d_u^2(\mathbf{P})(1 + n_u(\mathbf{P})/d_u(\mathbf{P}))} \left( d_u(\mathbf{P}) \frac{\partial n_u(\mathbf{P})}{\partial \mathbf{P}^*} - n_u(\mathbf{P}) \frac{\partial d_u(\mathbf{P})}{\partial \mathbf{P}^*} \right), \quad (42)$$

where  $\partial n_u(\mathbf{P})/\partial \mathbf{P}^* = [\partial n_u(\mathbf{P})/\partial \mathbf{p}_1^*, \dots, \partial n_u(\mathbf{P})/\partial \mathbf{p}_u^*]$  and  $\partial d_u(\mathbf{P})/\partial \mathbf{P}^* = [\partial d_u(\mathbf{P})/\partial \mathbf{p}_1^*, \dots, \partial d_u(\mathbf{P})/\partial \mathbf{p}_U^*]$ . Hence, to compute the gradient  $\nabla_{\mathbf{P}} R_{\text{sum}}(\mathbf{P})$ , we need to compute the derivatives of  $n_u(\mathbf{P})$  and  $d_u(\mathbf{P})$  for  $u = 1, \dots, U$ . We consider the third-order nonlinearity, i.e.,  $K = 1$  in (2) and accordingly  $\mathbf{G}(\mathbf{P})$  and  $\mathbf{C}_e(\mathbf{P})$  are as in (21) and (22), respectively. Starting with the numerator, it can be shown that the derivative with respect to  $\mathbf{p}_{u'}^*$  can be written as

$$\frac{\partial n_u(\mathbf{P})}{\partial \mathbf{p}_{u'}^*} = (\boldsymbol{\Gamma}_u(\mathbf{P}) \mathbf{1}_{\{u'=u\}}(u') + \boldsymbol{\Upsilon}_{u,u'}(\mathbf{P})) \mathbf{p}_{u'}, \quad (43)$$

for  $u' = 1, \dots, U$ , where  $\boldsymbol{\Gamma}_u(\mathbf{P}) \in \mathbb{C}^{B \times B}$  is given by

$$\begin{aligned} \boldsymbol{\Gamma}_u(\mathbf{P}) = & \mathbf{A}_1^* \mathbf{h}_u^* \mathbf{h}_u^T \mathbf{A}_1 + 2(\mathbf{A}_1^* \mathbf{h}_u^* \mathbf{h}_u^T \mathbf{A}_3 \text{diag}(\mathbf{P} \mathbf{P}^H) + \text{diag}(\mathbf{p}_u \mathbf{p}_u^H \mathbf{A}_1^* \mathbf{h}_u^* \mathbf{h}_u^T \mathbf{A}_3)) \\ & + 2(\text{diag}(\mathbf{P} \mathbf{P}^H) \mathbf{A}_3^* \mathbf{h}_u^* \mathbf{h}_u^T \mathbf{A}_1 + \text{diag}(\mathbf{A}_3^* \mathbf{h}_u^* \mathbf{h}_u^T \mathbf{A}_1 \mathbf{p}_u \mathbf{p}_u^H)) \\ & + 4(\text{diag}(\mathbf{P} \mathbf{P}^H) \mathbf{A}_3^* \mathbf{h}_u^* \mathbf{h}_u^T \mathbf{A}_3^* \text{diag}(\mathbf{P} \mathbf{P}^H) + \text{diag}(\mathbf{A}_3^* \mathbf{h}_u^* \mathbf{h}_u^T \mathbf{A}_3 \text{diag}(\mathbf{P} \mathbf{P}^H) \mathbf{p}_u \mathbf{p}_u^H \\ & + \mathbf{p}_u \mathbf{p}_u^H \text{diag}(\mathbf{P} \mathbf{P}^H) \mathbf{A}_3^* \mathbf{h}_u^* \mathbf{h}_u^T \mathbf{A}_3)). \end{aligned} \quad (44)$$

Furthermore,  $\Upsilon_u(\mathbf{P}) \in \mathbb{C}^{B \times B}$  can be expressed as

$$\begin{aligned} \Upsilon_{u,u'}(\mathbf{P}) = & 2(\text{diag}(\mathbf{p}_{u'} \mathbf{p}_{u'}^H \mathbf{A}_1^* \mathbf{h}_u^* \mathbf{h}_u^T \mathbf{A}_3) + \text{diag}(\mathbf{A}_1^* \mathbf{h}_u^* \mathbf{h}_u^T \mathbf{A}_3 \mathbf{p}_{u'} \mathbf{p}_{u'}^H)) \\ & + 4(\text{diag}(\mathbf{A}_3^* \mathbf{h}_u^* \mathbf{h}_u^T \mathbf{A}_3 \text{diag}(\mathbf{P} \mathbf{P}^H) \mathbf{p}_{u'} \mathbf{p}_{u'}^H) + \text{diag}(\mathbf{p}_{u'} \mathbf{p}_{u'}^H \text{diag}(\mathbf{P} \mathbf{P}^H) \mathbf{A}_3^* \mathbf{h}_u^* \mathbf{h}_u^T \mathbf{A}_3)). \end{aligned} \quad (45)$$

The derivative with respect to  $\mathbf{p}_{u'}^*$  of the denominator can be written as

$$\frac{\partial d_u(\mathbf{P})}{\partial \mathbf{p}_{u'}^*} = \frac{\partial d_u^{\text{mui}}(\mathbf{P})}{\partial \mathbf{p}_{u'}^*} + \frac{\partial d_u^{\text{dist}}(\mathbf{P})}{\partial \mathbf{p}_{u'}^*}, \quad (46)$$

where the derivative of the multiuser-interference term in the denominator is given by

$$\frac{\partial d_u^{\text{mui}}(\mathbf{P})}{\partial \mathbf{p}_{u'}^*} = \left( \mathbf{\Gamma}_u(\mathbf{P}) \mathbf{1}_{\{u' \neq u\}}(u') + \sum_{r \neq u} \Upsilon_{u,r}(\mathbf{P}) \right) \mathbf{p}_{u'}, \quad (47)$$

for  $u' = 1, \dots, U$ . Furthermore, the  $b$ th entry of the derivative of the nonlinear-distortion term in the denominator is given by

$$\begin{aligned} \frac{\partial d_u^{\text{dist}}(\mathbf{P})}{\partial p_{u',b}^*} = & 2 \left| \beta_3^{(b)} \right|^2 \left( 2 h_{u,b}^* \sum_{b'=1}^B h_{u,b'} p_{u',b'} \left[ |\mathbf{P} \mathbf{P}^H|^2 \right]_{b',b} \right. \\ & \left. + h_{u,b}^* \sum_{b'=1}^B h_{u,b'}^* p_{u',b'} \left[ (\mathbf{P} \mathbf{P}^H)^2 \right]_{b,b'} \right), \end{aligned} \quad (48)$$

for  $u' = 1, \dots, U$  and  $b = 1, \dots, B$ , where  $h_{b,u} = [\mathbf{h}_u]_b$ ,  $p_{b,u} = [\mathbf{p}_u]_b$  and  $\beta_3^{(b)}$  is the coefficient corresponding to the  $b$ th PA in the array. Finally, by inserting (40), (41), (43), (46), (47), and (48) into (42), we obtain a closed-form expression for the gradient  $\nabla_{\mathbf{P}} R_{\text{sum}}(\mathbf{P})$ .

## REFERENCES

- [1] S. Rezaei Aghdam, S. Jacobsson, and T. Eriksson, "Distortion-aware linear precoding for millimeter-wave multiuser MISO downlink," in *IEEE Int. Conf. Comm. (ICC) workshops*, Shanghai, China, May 2019.
- [2] E. Björnson, J. Hoydis, and L. Sanguinetti, "Massive MIMO networks: Spectral, energy, and hardware efficiency," *Found. Trends Signal Process.*, vol. 11, no. 3–4, pp. 154–655, Nov. 2017.
- [3] U. Gustavsson, C. Sánchez-Perez, T. Eriksson, F. Athley, G. Durisi, P. Landin, K. Hausmair, C. Fager, and L. Svensson, "On the impact of hardware impairments on massive MIMO," in *Proc. IEEE Global Commun. Conf. (GLOBECOM)*, Austin, TX, USA, Dec. 2014, pp. 294–300.
- [4] E. Björnson, J. Hoydis, M. Kountouris, and M. Debbah, "Massive MIMO systems with non-ideal hardware: Energy efficiency, estimation, and capacity limits," *IEEE Trans. Inf. Theory*, vol. 11, no. 60, pp. 7112–7139, Nov. 2014.
- [5] A. Papazafeiropoulos, B. Clerckx, and T. Ratnarajah, "Rate-splitting to mitigate residual transceiver hardware impairments in massive MIMO systems," *IEEE Trans. on Veh. Technol.*, vol. 66, no. 9, pp. 8196–8211, Sep. 2017.
- [6] M. Abdelghany, A. A. Farid, U. Madhow, and M. J. W. Rodwell, "A design framework for all-digital mmwave massive MIMO with per-antenna nonlinearities," Dec. 2019. [Online]. Available: <https://arxiv.org/abs/1912.11643>
- [7] J. Qi and S. Aissa, "On the power amplifier nonlinearity in MIMO transmit beamforming systems," *IEEE Trans. Commun.*, vol. 60, no. 3, pp. 876–887, Mar. 2012.
- [8] S. Blandino, C. Desset, A. Bourdoux, L. Van der Perre, and S. Pollin, "Analysis of out-of-band interference from saturated power amplifiers in massive MIMO," in *Proc. Eur. Conf. Netw. Commun. (EuCNC)*, Oulu, Finland, Jul. 2017.
- [9] C. Mollén, U. Gustavsson, T. Eriksson, and E. G. Larsson, "Spatial characteristics of distortion radiated from antenna arrays with transceiver nonlinearities," *IEEE Trans. Wireless Commun.*, vol. 17, no. 10, pp. 6663–6679, Oct. 2018.
- [10] N. N. Moghadam, G. Fodor, M. Bengtsson, and D. J. Love, "On the energy efficiency of MIMO hybrid beamforming for millimeter-wave systems with nonlinear power amplifiers," *IEEE Trans. Wireless Commun.*, vol. 17, no. 11, pp. 7208–7221, Nov. 2018.
- [11] M. R. Khanzadi, G. Durisi, and T. Eriksson, "Capacity of SIMO and MISO phase-noise channels with common/separate oscillators," *IEEE Trans. Commun.*, vol. 63, no. 9, pp. 3218–3231, Sep. 2015.
- [12] N. Kolomvakis, M. Matthaiou, and M. Coldrey, "IQ imbalance in multiuser systems: Channel estimation and compensation," *IEEE Trans. Commun.*, vol. 64, no. 7, pp. 3039–3051, Jul. 2016.
- [13] S. Jacobsson, G. Durisi, M. Coldrey, T. Goldstein, and C. Studer, "Quantized precoding for massive MU-MIMO," *IEEE Trans. Commun.*, vol. 65, no. 11, pp. 4670–4684, Nov. 2017.
- [14] X. Zhang, M. Matthaiou, M. Coldrey, and E. Björnson, "Impact of residual transmit RF impairments on training-based MIMO systems," *IEEE Trans. Commun.*, vol. 63, no. 8, pp. 2899–2911, Aug. 2015.
- [15] A. Papazafeiropoulos, S. K. Sharma, T. Ratnarajah, and S. Chatzinotas, "Impact of residual additive transceiver hardware impairments on rayleigh-product MIMO channels with linear receivers: Exact and asymptotic analyses," *IEEE Trans. Commun.*, vol. 66, no. 1, pp. 105–118, 2018.
- [16] C. Studer, M. Wenk, and A. Burg, "MIMO transmission with residual transmit-RF impairments," in *Proc. Int. ITG Workshop on Smart Antennas (WSA)*, Bremen, Germany, Feb. 2010, pp. 189–196.
- [17] E. G. Larsson and L. Van der Perre, "Out-of-band radiation from antenna arrays clarified," *IEEE Wireless Commun. Lett.*, vol. 7, no. 4, pp. 610–613, Feb. 2018.
- [18] L. Anttila, A. Brihuega, and M. Valkama, "On antenna array out-of-band emissions," *IEEE Wireless Commun. Lett.*, vol. 8, no. 6, pp. 1653–1656, Dec 2019.

- [19] S. Jacobsson, U. Gustavsson, G. Durisi, and C. Studer, “Massive MU-MIMO-OFDM uplink with hardware impairments: Modeling and analysis,” in *Proc. Asilomar Conf. Signals, Syst., Comput.*, Pacific Grove, CA, USA, Oct. 2018, pp. 1829–1835.
- [20] E. Björnson, L. Sanguinetti, and J. Hoydis, “Hardware distortion correlation has negligible impact on UL massive MIMO spectral efficiency,” *IEEE Trans. Commun.*, vol. 67, no. 2, pp. 1085–1098, Feb. 2019.
- [21] S. R. Aghdam and T. Eriksson, “On the performance of distortion-aware linear receivers in uplink massive MIMO systems,” in *Proc. IEEE Int. Symp. Wirel. Comm. Syst. (ISWCS)*, Oulu, Finland, Aug. 2019, pp. 208–212.
- [22] O. T. Demir and E. Björnson, “Channel estimation in massive MIMO under hardware non-linearities: Bayesian methods versus deep learning,” *IEEE Open J. Commun. Soc.*, vol. 1, pp. 109–124, 2020.
- [23] J. J. Bussgang, “Crosscorrelation functions of amplitude-distorted Gaussian signals,” Res. Lab. Elec., Cambridge, MA, USA, Tech. Rep. 216, Mar. 1952.
- [24] T. Schenk, *RF imperfections in high-rate wireless systems: Impact and digital compensation*. Dordrecht, The Netherlands: Springer-Verlag, 2008.
- [25] D. Persson, T. Eriksson, and E. G. Larsson, “Amplifier-aware multiple-input multiple-output power allocation,” *IEEE Commun. Lett.*, vol. 17, no. 6, pp. 1112–1115, 2013.
- [26] A. Grebennikov, *RF and microwave power amplifier design*. McGraw-Hill New York, 2005.
- [27] S. N. Diggavi and T. M. Cover, “The worst additive noise under a covariance constraint,” *IEEE Trans. Inf. Theory*, vol. 47, no. 7, pp. 3072–3081, Nov. 2001.
- [28] D. P. Palomar and S. Verdú, “Gradient of mutual information in linear vector gaussian channels,” *IEEE Trans. Inf. Theory*, vol. 52, no. 1, pp. 141–154, 2005.
- [29] D. Feng, C. Jiang, G. Lim, L. J. Cimini, G. Feng, and G. Y. Li, “A survey of energy-efficient wireless communications,” *IEEE Commun. Surv. Tut.*, vol. 15, no. 1, pp. 167–178, 2013.
- [30] A. Alkhateeb, O. El Ayach, G. Leus, and R. W. Heath Jr., “Channel estimation and hybrid precoding for millimeter wave cellular systems,” *IEEE J. Sel. Topics Signal Process.*, vol. 8, no. 5, pp. 831–846, Oct. 2014.
- [31] A. Alkhateeb, G. Leus, and R. W. Heath Jr., “Limited feedback hybrid precoding for multi-user millimeter wave systems,” *IEEE Trans. Wireless Commun.*, vol. 14, no. 11, pp. 6481–6494, Nov. 2015.
- [32] M. R. Akdeniz, Y. Liu, M. K. Samimi, S. Sun, S. Rangan, T. S. Rappaport, and E. Erkip, “Millimeter wave channel modeling and cellular capacity evaluation,” *IEEE J. Sel. Areas Commun.*, vol. 32, no. 6, pp. 1164–1179, Jun. 2014.
- [33] E. Björnson, L. Sanguinetti, and J. Hoydis, “Can hardware distortion correlation be neglected when analyzing uplink SE in massive MIMO?” in *Proc. IEEE Int. Workshop Signal Process. Advances Wireless Commun. (SPAWC)*, Kalamata, Greece, Jun. 2018.
- [34] C. Mollén, U. Gustavsson, T. Eriksson, and E. G. Larsson, “Impact of spatial filtering on distortion from low-noise amplifiers in massive MIMO base stations,” *IEEE Trans. Commun.*, vol. 66, no. 12, pp. 6050–6067, 2018.